Article

Micro- and Macro- Mechanical Properties of Thermoelectric Lead Chalcogenides

Guodong Li, Umut Aydemir, Bo Duan, Matthias Agne, Hongtao Wang, Max Wood, Qingjie Zhang, Pengcheng Zhai, William A. Goddard, and G. Jeffrey Snyder

ACS Appl. Mater. Interfaces, **Just Accepted Manuscript** • DOI: 10.1021/acsami.7b15651 • Publication Date (Web): 03 Nov 2017

Micro- and Macro- Mechanical Properties of Thermoelectric Lead Chalcogenides

Guodong Li [†,‡], Umut Aydemir [‡,§], Bo Duan [†], Matthias T. Agne [‡], Hongtao Wang [†], Max Wood [‡], Qingjie Zhang [*,†], Pengcheng Zhai [†], William A. Goddard III [⊥], and G. Jeffrey Snyder [*,‡]

[†]State Key Laboratory of Advanced Technology for Materials Synthesis and Processing, Wuhan University of Technology, Wuhan 430070, China.

[‡]Department of Materials Science and Engineering, Northwestern University, Evanston, Illinois 60208, USA.

[§] Department of Chemistry, Koc University, Sariyer, Istanbul 34450, Turkey

[⊥]Materials and Process Simulation Center, California Institute of Technology, Pasadena, California 91125, USA.

[*]Corresponding authors: jeff.snyder@northwestern.edu; zhangqj@whut.edu.cn

Abstract: Both n- and p-type lead telluride (PbTe) based thermoelectric (TE) materials display high thermoelectric efficiency, but the low fracture strength may limit their commercial applications. In order to find ways to improve these macroscopic mechanical properties we report here the ideal strength and deformation mechanism of PbTe using density functional theory (DFT) calculations. This provides structure-property relationships at the atomic scale that can be applied to estimate macroscopic mechanical properties such as fracture toughness. Among all the shear and tensile paths that examined here, we find the lowest ideal strength of PbTe is 3.46 GPa along the (001)/<100> slip system. This leads to an estimated fracture toughness of 0.28 MPa $m^{1/2}$ based on its ideal stress-strain relation, which is in good agreement with our experimental measurement of 0.59 MPa $m^{1/2}$. We find that softening and breaking of the ionic Pb–Te bond leads to the structural collapse. To improve the mechanical strength of PbTe, we suggest strengthening the structural stiffness of the ionic Pb–Te framework through an alloying strategy, such as alloying PbTe with isotypic PbSe or PbS. This point defect strategy has a great potential to develop high-performance PbTe based materials with robust mechanical properties, which may also be applied to other materials and applications.

1. INTRODUCTION

The rapid depletion of fossil fuels is giving rise to severe environmental impact including global climate change, which urgently demands development of renewable energy technologies. Because thermoelectric (TE) power generation devices can convert waste heat generated *e.g.*, from home heating, automotive exhaust, and industrial process into electricity, TE waste heat recovery technology could make a significant contribution to global sustainable energy solutions.[1] Indeed the past two decades has seen dramatic enhancements in the TE figure of merit, $zT = \alpha^2\sigma/\kappa$, of various materials, achieved through simultaneously optimizing the power factor ($\alpha^2\sigma$) and reducing the thermal conductivity[2] for such materials as PbTe,[3-5] skutterudite $CoSb_3$,[6-8] Bi_2Te_3,[9-11] Mg_2Si,[12-13] and half-Heusler alloys.[14,15] However, despite the improved efficiencies, applications of these TE materials usually impose a severe cyclic temperature gradients that can generate cracks in the microstructure.[16,17] Such cracks lead to deterioration in the material performance, accelerating failure processes of these TE devices upon cycling.[16,17] In order to improve these mechanical properties, it is important to gain an understanding of the mechanical strength and toughness of these TE materials so that TEs with improved performance can be developed for engineering applications.

PbTe, the most widely studied TE material, is one of the best performing TE semiconductors for power generation at intermediate temperatures.[2,3,18] Because both n- and p-type PbTe exhibit exceptional TE performances,[3-5,18] it has been used in TE generators on space missions since the 1960s.[1] In terms of mechanical properties, Li *et al.* studied creep deformation and found PbTe has a good hot ductility compared to Bi_2Te_3.[19] Petersen *et al.* studied the bulk modulus, shear modulus, and Young's modulus of PbTe and PbSe using first-principle calculations, and estimated the brittleness of PbTe.[20] Ni *et al.* experimentally reported the room temperature Young's modulus, shear modulus, Poisson's ratio, and Vicker's hardness of PbTe nanostructured material.[21] Gelbstein *et al.* found that n-type PbTe is much stronger in its bending strength and more ductile than p-type PbTe.[22] They also discussed the microhardness enhancement of p-type PbTe alloys with hole concentrations higher than 5×10^{18} cm^{-3},[23] which agrees well with Zlatanov's experimental observation.[24] Cui *et al.* prepared the binary alloys $(PbTe)_{1-x}(SnTe)_x$ over the whole composition range and found that alloys with mole fraction x ranging from 0.2 to 0.6 have the highest compression strengths (310 – 330 MPa) and hardness (HV95).[25] Nevertheless, the failure mechanism of PbTe, and its intrinsic mechanical properties remain unknown so far.

To determine the deformation mechanism and understand the intrinsic mechanical properties of PbTe, we used density functional theory (DFT) with the Perdew–Burke–Ernzerhof (PBE)

functional to investigate the response for pure and biaxial shear deformations of single-crystalline PbTe. Under pure shear deformations, we find that PbTe has the lowest ideal shear strength of 3.46 GPa along the (001)/<100> slip system, suggesting this to be the most likely slip system activated under pressure. This value is lower than the ideal tensile strength (5.55 GPa) of PbTe along the [100] tension. This is because the ionic Pb–Te bond in the 3D Pb–Te framework is distorted to resist the deformation. Further deformation leads to the softening and breakage of these ionic bonds. Compression plays a significant role in PbTe's mechanical strength. We find that PbTe has an ideal strength of 2.96 GPa under biaxial shear deformation (relevant for indentation measurements of hardness), which is lower than that of the pure shear deformation (3.46 GPa). We also find that both isostructural PbSe and PbS have higher structural stiffness than PbTe in resisting deformation, leading to a high ideal shear strength of 5.13 GPa in PbSe and 7.14 GPa in PbS. Moreover, estimating the fracture toughness from the ideal stress-strain curves, we find that the fracture toughness increases in the order PbTe (K_{IIc} = 0.23 MPa $m^{1/2}$) < PbSe (K_{IIc} = 0.33 MPa $m^{1/2}$) < PbS (K_{IIc} = 0.41 MPa $m^{1/2}$). This trend shows a good agreement with our experimental results, PbTe (K_{Ic} =0.59±0.02 MPa $m^{1/2}$) < PbSe (K_{Ic} = 0.67±0.05 MPa $m^{1/2}$) < PbS (K_{Ic} = 0.75±0.04 MPa $m^{1/2}$), which is in parallel with the structural resistance argument of Pb–Te (stretching force constant, SFC = 0.291 eV/ $Å^2$) < Pb–Se (SFC = 0.397 eV/ $Å^2$) < Pb–S (SFC = 0.502 eV/ $Å^2$). This suggests that strengthening the structural stiffness of the ionic Pb–Te framework by alloying with isotypic PbSe or PbS may improve the mechanical strength of PbTe. We aim to provide essential information in understanding the intrinsic mechanical behavior of PbTe. This ideal structure – property relation could be useful for predicting how to design high-performance TE materials with robust mechanical properties.

2. METHODOLOGY

2.1 Calculation methods

All DFT calculations were performed by the Vienna *ab initio* Simulation Package (VASP) periodic code with plane-wave basis sets.[26-28] The Perdew-Burke-Ernzerhof (PBE) functional is used to include electronic exchange-correlation, and the projector augmented wave (PAW) method is used to include the core-valence interactions. Our convergence tests showed that an energy cutoff of 500 eV gives an excellent convergence on energy, force, and geometries. The convergence for the electronic self-consistent field and the force criterion were set to 1×10^{-6} eV

and 1×10^{-2} eV/Å, respectively. All calculations used the Γ-centered Monkhorst-Pack scheme with a fine resolution of $2\pi\times1/40$ Å^{-1} in the *k*-point reciprocal space sampling. The electron localization function (ELF) was calculated to help understand the chemical bonding.

The elastic constants, C_{ij}, were computed from stress - strain relationship as a function of various cell distortions, δ ($\delta < 3\%$), starting with our optimized atomic structure. The inverse of the elasticity tensor, S_{ij}, was derived from $S_{ij} = (C_{ij})^{-1}$. Subsequently, the Voigt-Reuss-Hill method was applied to calculate the isotropic polycrystalline elastic moduli from the calculated single-crystal elastic constants.[29]

To examine shear deformations, we achieved quasi-static mechanical loading by imposing a shear strain for one particular shear plane while allowing full structural relaxation along the other five strain components.[30] To mimic the experimental indentation process, we applied biaxial shear deformation by considering the normal compressive pressure beneath the indenter and constraining the ratios of normal stress (σ_{zz}) to shear stress (σ_{xz}) as $\sigma_{zz} = \sigma_{xz}\tan\phi$, where $\phi = 68^{o}$ for a Vickers indenter.[31] The residual stresses are all less than 0.5 GPa for both pure and biaxial shear deformations.

2.2 Experimental methods

Polycrystalline samples of PbTe, PbSe and PbS were synthesized via a solid-state reaction followed by high temperature - high pressure (HTHP) method. The stoichiometric amounts of powders of Pb (99.99%, Alfa Aesar), Te (99.999%, Alfa Aesar), Se (99.9%, Alfa Aesar) and S (99.9%, Alfa Aesar) were hand mixed in an agate mortar and sealed into quartz ampoules under vacuum. The sealed ampoules were then slowly heated up to 1203 K (PbTe), 1323 K (PbSe), and 1323 K (PbS) for 2 h, and then cooled down to 1123 K in 6 h (PbTe) and 8 h (PbSe and PbS). Finally, all the ampoules were cooled from 1123 K to room temperature during a 5 h period. The obtained materials were then compacted using HTHP at 773 K for 10 min under 2 GPa. The crystal structure and purity of samples was confirmed using an X-ray diffractometer with Cu K_α radiation.

Fracture toughness (K_{IC}) was measured using the three point flexural specimen by the single-edge notch beam test (Zwick Z005 HT). The tested bars were cut from the HTHP-processed samples with the same nominal dimensions 12 × 3 × 1.5 mm, the span was set at 7 mm, and the testing was conducted at a cross-head speed of 0.05 mm/min. The starting notch with a

length of half the width was created at the mid-span of the sample, and the width of the notch was less than 0.2 mm.

K_{IC} was calculated via Eqn. 1,

$$K_{IC} = \frac{3PL\sqrt{a \times 10^{-3}}}{2BW^2}\left[1.93 - 3.07\left(\frac{a}{W}\right) + 14.53\left(\frac{a}{W}\right)^2 - 25.07\left(\frac{a}{W}\right)^3 + 25.80\left(\frac{a}{W}\right)^4\right] \quad \text{Eqn. 1}$$

Where P, L, b, w and a are the applied load, span, beam thickness, beam height and depth of starting notch, respectively.

3. RESULTS AND DISCUSSION

3.1 Crystal Structure and Chemical Bonding in PbTe

The IV-VI binary compound PbTe has the face centered cubic lattice (NaCl structure type), crystallizing in the *Fm*-3*m* (225) space group.[33] Figure 1 displays the unit cell of PbTe containing 4 × Pb and 4 × Te atoms along with the calculated electron localization function (ELF). The ELF shows efficient charge transfer occurs between Pb and Te atoms (few shared electrons), indicating primarily ionic bonding character with a bond length of 3.28 Å. The electrons around Te atoms are described as lone pair *p* orbitals. The optimized lattice parameter is a = 6.56 Å, which is only 1.5% larger than the experimental value of 6.46 Å[33] at 298K, and is in good agreement with the theoretical value of 6.57 Å from previous DFT calculations based on the PBE functional.[34]

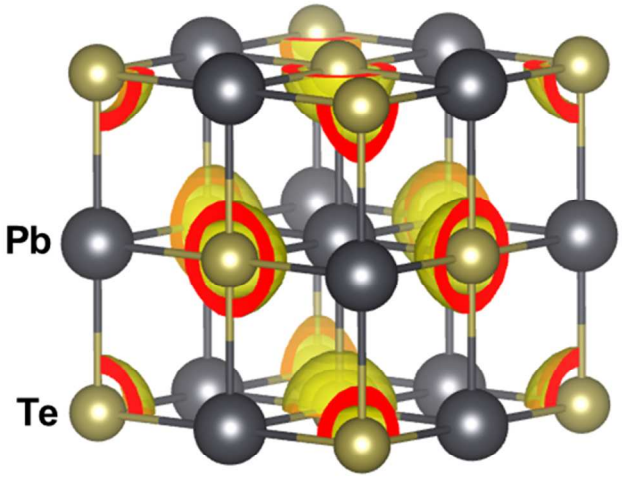

Figure 1. Crystal structure of PbTe with calculated isosurfaces (at the value of 0.85) for the electron localization function (ELF). The Electron localization function (ELF) value, which ranges from 0 to 1, enables an effective and reliable analysis of bonding character and lone pair formation.[32] The Pb–Te bonding interaction with the length of 3.28 Å is considered to be ionic. The electrons around Te atoms are described as lone pair *p* orbitals. The Pb and Te atoms are represented with gray and brown spheres, respectively.

3.2 Elastic Properties in PbTe

To determine the structure – property relation of PbTe, we studied the elastic mechanical properties to provide essential information on the structural stability, as listed in Table 1. The predicted elastic constants, C_{ij}, agree well with previous theoretical values.[34] Using Voigt–Reuss–hill method, the calculated bulk modulus B = 38.62 GPa, the shear modulus G = 24.13 GPa, the Young's modulus E = 59.91 GPa, the Poisson's ratio v = 0.241, and the ductility ratio B/G = 1.60, were calculated and listed in Table 1. Our calculated elastic moduli of PbTe agree well with the experimental values,[21,35,36] but are much lower than those of other TE materials such as $CoSb_3$ (B = 87.38 GPa, G = 59.45 GPa, E = 145.38 GPa) and TiNiSn (B = 128.78 GPa, G = 67.16 GPa, E = 171.65 GPa).[37,38] This suggests that PbTe has a significantly lower structural stiffness than $CoSb_3$ and TiNiSn. In addition, we also investigated the elastic mechanical properties of PbSe and PbS, as listed in Table 1. PbSe and PbS have a higher and much higher elastic modulus compared with PbTe, respectively, which we attribute to the

stronger and much stronger bond stiffness of Pb–Se (the stretching force constant, SFC = 0.397 eV/ Å^2) and Pb–S (SFC = 0.502 eV/ Å^2) compared with Pb–Te (SFC = 0.291 eV/ Å^2), as discussed in Section 3.5.

Table 1. Predicted elastic constants (C_{11}, C_{12}, C_{44}), bulk modulus (B), shear modulus (G), Young's modulus (E), Poisson's ratio (v), and ductility ratio (B/G) of PbTe, PbSe, and PbS, and previous experimental and theoretical values.

		Method	C_{11} (GPa)	C_{12} (GPa)	C_{44} (GPa)	B (GPa)	G (GPa)	E (GPa)	v	B/G
PbTe	This study	PBE	105.18	5.34	14.13	38.62	24.13	59.91	0.241	1.60
	Ref. 34	PBE	108	6	14	40	24	51.43	0.25	1.67
	Ref. 21	Expt	-	-	-	-	22.32	57.5	0.243	-
	Ref. 35	Expt	-	-	-	-	-	59	-	-
	Ref. 20	PBE	-	-	-	39.1	-	-	-	-
	Ref. 36	Expt	-	-	-	38.39	-	-	-	-
PbSe	This study	PBE	119.19	12.76	17.5	48.24	27.85	70.07	0.258	1.73
	Ref. 34	PBE	117	12	17	47	27	68.51	0.26	1.73
PbS	This study	PBE	130.42	17.26	19.63	54.98	30.49	77.20	0.266	1.80
	Ref. 34	PBE	121	18	20	52	29	74.58	0.26	1.77

3.3 Shear Deformation and Failure Mechanism of PbTe

The elastic properties listed in Table. 1 describe the mechanical properties for small strains less than 3%. This is not sufficient to account for the mechanical strength and failure mechanism nor the bonding characteristics at larger strains. To determine the ideal strength and deformation mechanism of PbTe, we applied pure shear deformation to examine the stress response along various slip directions. We considered three typical slip systems, (001)/<100>, (111)/<1-10>, and (111)/<11-2> with supercells containing 64, 48, and 48 atoms, respectively. Figure 2(a) displays the shear-stress – shear-strain relationships for these slip systems. Shear stress in all three systems increases linearly with increasing shear strain, indicating each of these slip systems uniformly resists the shear deformation. The slope of the (001)/<100> slip system is much lower than the other two slip systems, indicating a much lower structural stiffness in resisting external deformation along the (001)/<100> direction. From the elastic shear-stress – shear-strain region

along the (001)/<100> direction, we obtained the directional shear moduli G_{xy} = 14.10 GPa. This value agrees well with the elastic constant C_{44} of 14.13 GPa listed in Table 1. (001)/<100> is found to have the lowest ideal shear strength of 3.46 GPa at 0.277 shear strain, while (111)/<1-10> and (111)/<11-2> have a higher ideal strength of 4.54 GPa at 0.232 shear strain and 6.22 GPa at 0.358 shear strain, respectively. This suggests that the most plausible slip plane for PbTe is (001)/<100>. Beyond this maximum stress point, the shear-stress drops suddenly both in the (111)/<1-10> and (111)/<11-2> directions, indicating structural collapse and failure. However, there is an obvious 'yielding' process in the (001)/<100> direction, suggesting a softening structural stiffness.

To understand these behaviors, we need to understand the detailed deformation and failure mechanisms, shown in Figure 2(b)-(d) and Figure S1-S2 in the Supporting Information (SI). First, we extracted the atomic configurations at the critical strains, finding the Pb–Te bond length changes in the (001)/<001> direction (Figure 2(b)-(d)). During the whole shear process, the Pb-Te ionic framework is maintained (Figure 2(b)-(c)). The Pb–Te bonds along the *a* and *c* axes are stretched, but the Pb–Te bonds along the *b* axis shrink to resist the deformation (Figure 2(d)). As the shear strain increases to 0.277, corresponding to the ideal shear strength, Pb–Te bonds along the *a* and *c* axes have stretched from 3.28 to 3.33 Å, a stretching ratio of 1.53%, while the Pb–Te bonds along the *b* axis shrink from 3.28 to 3.26 Å, a shrinking ratio of 0.7%. With increasing shear strain, the Pb–Te bonds along the *b* axis remain nearly unchanged, but the Pb–Te bonds along the *a* and *c* axes increase rapidly to 3.41 Å, suggesting a gradual softening of the Pb–Te bonds. This leads to the 'yielding' stage, as shown in Figure 2(a). Figure S1 shows the shear deformation of PbTe along the (111)/<1-10> direction. The structure distorts to resist the deformation until 0.266 shear strain beyond which it fails (Figure S1(a)-(b)). At the failure strain of 0.277, the structure displays significant atomic rearrangements, relaxing the shear stress and leading to the structural failure (Figure S1(c)). Before the failure, the Pb–Te(1) bond has stretched from 3.28 to 3.49 Å with a stretching ratio of 6.4%, while the Pb–Te(2) bond shrinks from 3.28 to 3.21 Å with a shrinking ratio of 2.1% (Figure S1(d)). At the failure strain of 0.277, the Pb–Te(1) bond recovers to 3.26 Å, and the Pb–Te(2) bond increases sharply to 3.89 Å. Such a long distance indicates breaking of the Pb–Te(2) bond, which leads to the structural rearrangement and stress relaxation. This deformation mechanism is also observed in PbTe for shearing along the (111)/<11-2> direction, as shown in Figure S2.

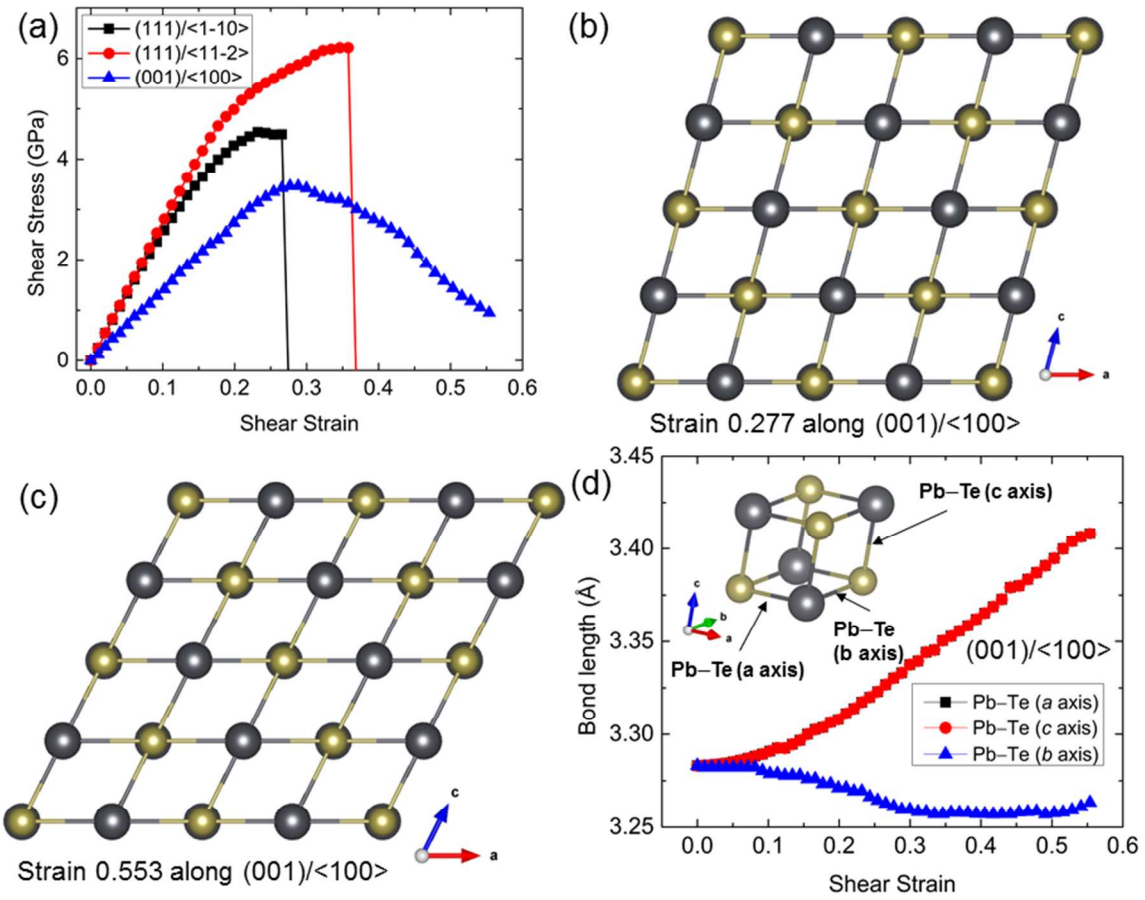

Figure 2. The ideal shear strength and shear deformation mechanism of PbTe. (a) The shear-stress−shear-strain relationships for PbTe under shear deformation along various slip systems. The atomic structures of PbTe shearing along the (001)/<100> slip system: (b) Structure at 0.277 shear strain corresponding to the ideal shear strength, (c) Structure at 0.553 shear strain corresponding to the highly softening Pb–Te ionic framework. (d) The average bond lengths of Pb–Te with the increasing shear strain along the (001)/<100> slip system. The Pb and Te atoms are represented with gray and brown spheres, respectively. The substructure embedded in Figure 2(d) highlights the Pb–Te bonds along different directions.

3.4 Tensile Deformation and Failure Mechanism of PbTe

To further understand the failure mechanism of PbTe, we investigated the tensile stress response under different tensile loads, as displayed in Figure 3. We considered three typical tensile systems, [100], [1-10], and [111] with supercells containing 64, 48, and 48 atoms, respectively. Figure 3(a) shows the tensile-stress – tensile-strain relations. The lowest ideal tensile strength is found to be 5.55 GPa at 0.138 tensile strain along the [100] direction, which is lower

than the maximum tensile stress of 6.84 GPa and 8.39 GPa along the [1-10] and [111] direction, respectively. In addition, the lowest ideal tensile strength (5.55 GPa) is higher than the lowest ideal shear strength (3.46 GPa) along the (001)/<100> slip system, which suggests that shear deformations occur more easily than tensile deformations. Tension along the [100] direction shows an obvious 'yielding' process, which is similar to shearing along the (001)/<100> direction as discussed above, while tensions along both the [1-10] and [111] directions show a sudden drop in tensile stress. We extracted the structural and bond length changes at critical tensile strains to determine the bond-responding processes, as displayed in Figure 3(b)-(d) and Figure S3-S4 in the SI. For tension along the [100] direction, as the tensile strain increases to 0.138 which corresponds to the ideal tensile stress, no bond breaks as shown in Figure 3(b). The Pb–Te bonds along the *a* axis stretch uniformly from 3.28 to 3.73 Å with a stretching ratio of 13.7%, while the Pb–Te bonds along the *b* and *c* axes both shrink slightly to coordinate the tensile deformation along the *a* (or [100]) direction with a shrinking ratio of 0.8% (Figure 3(d)). With further increasing tensile stress, the Pb–Te bonds along the *a* axis start to soften, leading to a weakened Pb–Te ionic framework and a lower tensile stress. At 0.662 tensile strain, the Pb–Te bond length (*a* axis) gradually increases to 5.45 Å, indicating a highly softened or non-bonding interaction (Figure 3(c)). This "yielding" process gradually weakens the structural stiffness, releasing the tensile stress, as shown in Figure 3(a). For tension along the [1-10] direction as shown in Figure S3, the Pb–Te(1) bond is stretched and the Pb–Te(2) bond is shrank to resist tensile deformation. At 0.220 tensile strain, the Pb–Te(1) and Pb–Te(2) bond length increases and decreases to 3.49 and 3.25 Å, respectively, representing the maximum resistance to tensile deformation. As the tensile strain increases further, the sudden decrease of the Pb–Te(1) bond at 0.232 and 0.257 tensile strains decreases the structural stiffness, leading to the sudden drop of the tensile stress as shown in Figure 3(a). For tension along the [111] direction (Figure S4), the Pb–Te(1) and Pb–Te(2) bonds are both stretched to resist the deformation until the maximum tensile stress point. The breaking of the Pb–Te(1) bond collapses the structure, leading to the failure of PbTe.

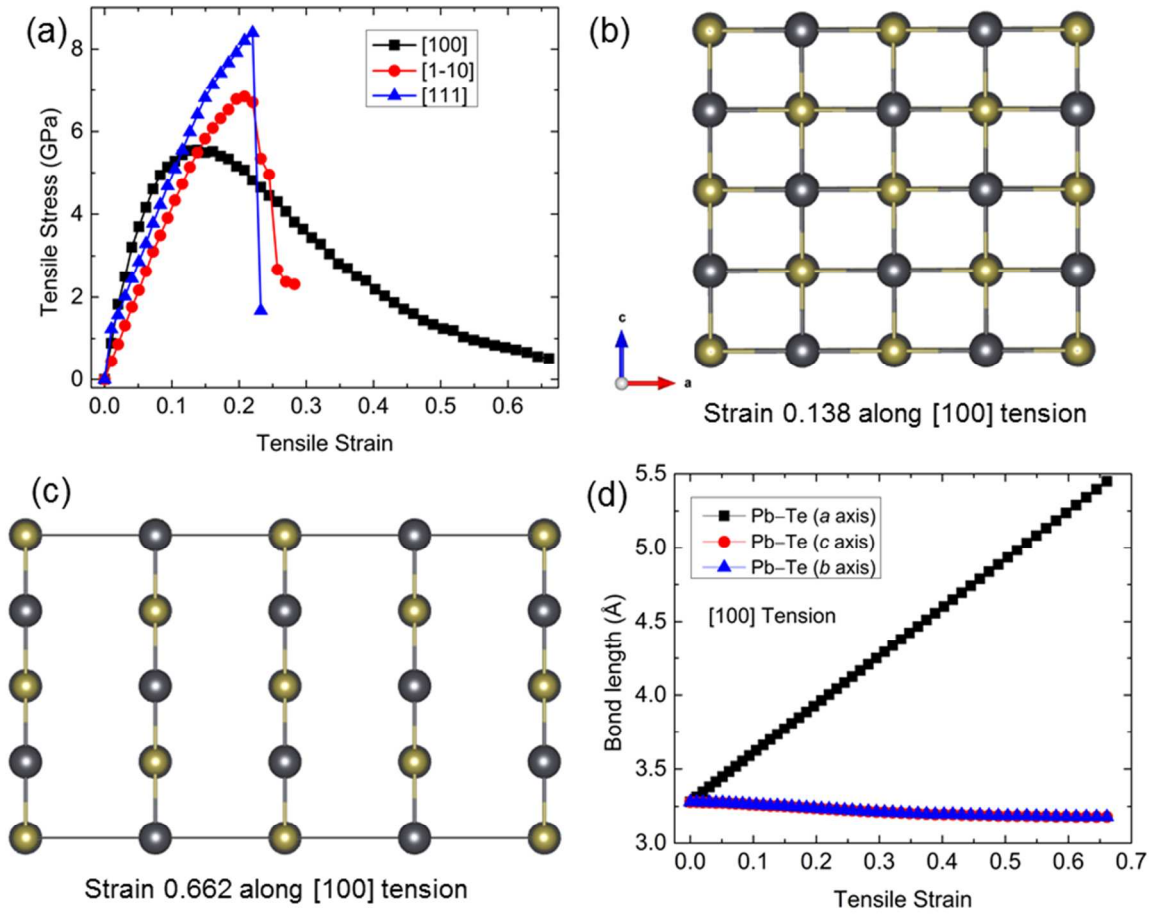

Figure 3. The ideal tensile strength and tensile deformation mechanism of PbTe. (a) The tensile-stress−tensile-strain relationships for PbTe under various tensile loads. The atomic structures of PbTe along the [100] direction: (b) Structure at 0.138 tensile strain corresponding to the ideal tensile strength, (c) Structure at 0.662 tensile strain corresponding to the highly softening Pb–Te ionic framework. (d) The average bond lengths of Pb–Te with the increasing tensile strain along the [100] direction. The Pb and Te atoms are represented with gray and brown spheres, respectively.

3.5 Effect on Ideal Strength of PbTe by Alloying

The ideal strength, which reflects the structural resistance limitation on external deformation, plays a significant role in determining the reliability of a material.[39] The structure of PbTe is comprised of an ionic 3D Pb–Te framework. The ionic Pb–Te bond dominates the ideal strength of PbTe, and the softening and the breaking of these bonds lead to structural failure. The ideal shear strength (3.46 GPa) of PbTe is higher than those of layered TE materials such as Mg_3Sb_2 (1.95 GPa) and SnSe (0.59 GPa),[40,41] but it is much lower than those of 3D TE materials with

strong covalent frameworks such as $CoSb_3$ (7.17 GPa) and TiNiSn (10.52 GPa).[37,38] The PbTe compound shows an extremely high *zT* value experimentally.[3,4] However, its ideal strength is relatively low. For engineering applications of PbTe, the structural rigidity of the ionic Pb–Te framework should be enhanced to improve its mechanical integrity.

To determine the effect of structural rigidity on the ideal strength of PbTe, we calculated the shear-stress – shear strain relations of isotypic PbSe and PbS along the most likely slip system of (001)/<100>, as shown in Figure 4(a). PbSe and PbS have higher ideal shear strengths of 5.13 GPa and 7.04 GPa, respectively, compared with that of PbTe (3.46 GPa). In addition, PbSe and PbS have a similar deformation mechanism as PbTe (see Figure S5-S6 in the SI). This suggests that alloying PbTe with PbSe or PbS may be an effective way to improve the mechanical properties of PbTe. Moreover, we also calculated the structural rigidity, as proposed in our previous study,[37] to understand quantitatively how the structure influences the ideal strength, as shown in Figure 4(b). The "maximum structural resistance (Δ)" is defined as $\Delta=\sum_i k_i n_i \left| l^i - l_0^i \right|$, where *i* represents the bond type in the compound, k_i is the stretching force constant (SFC) of the *i* bond which can be calculated by the ATAT code,[42] n_i is the weight of the *i* bond which is determined by the number of the bond in the unit cell. l_0^i is the length of the *i* bond at equilibrium state, and l^i is the length of the *i* bond at the critical strain corresponding to the ideal strength. PbTe has a lower SFC and bond deformation $\left| l^i - l_0^i \right|$ (0.291 eV/ Å^2 and 0.069 Å) compared with those of PbSe (0.397 eV/ Å^2 and 0.089 Å) and PbS (0.502 eV/ Å^2 and 0.128 Å). This leads to a higher "maximum structural resistance" in PbSe and PbS than PbTe (Figure 4(b). To improve the mechanical properties of PbTe, we suggest strengthening the Pb–Te ionic framework to improve the "maximum structural resistance" through an alloying strategy such as the partial substituting Te with Se or S.

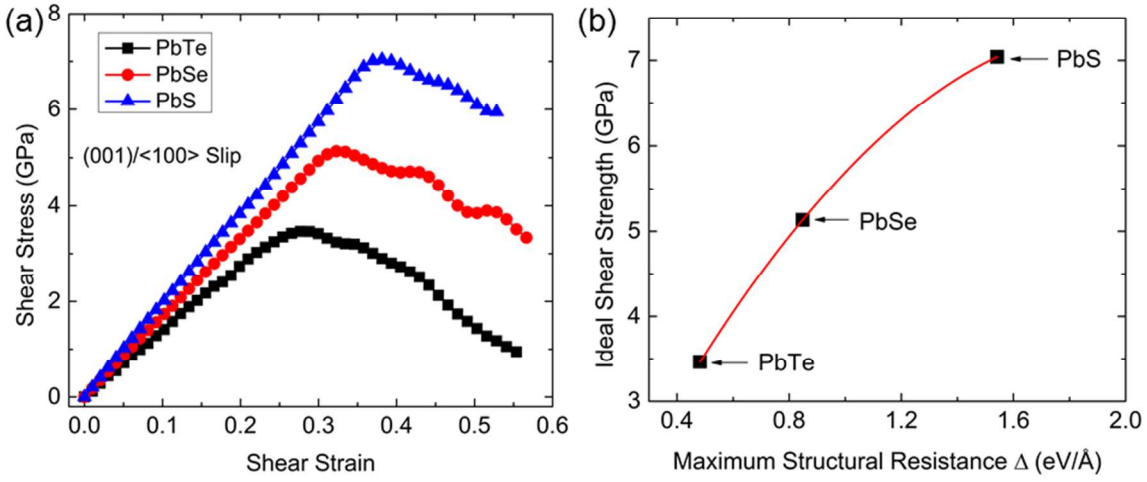

Figure 4. Effect of alloying on the ideal shear strength of PbTe. (a) The shear-stress − shear-strain relationships for isotypic PbTe, PbSe, and PbS along the (001)/<100> slip system. (b) Predicted ideal shear strength as a function of the proposed "Maximum structural resistance, Δ". The unit of Δ is eV/ Å. The red line is a guide to the eye.

3.6 Failure Mechanism of PbTe under Biaxial Shear Deformation

To mimic the complex stress conditions for indentation experiments, we imposed biaxial shear deformation in determining the underlying failure mechanism of PbTe. The computed shear-stress – shear-strain relations for biaxial shear deformation are shown in Figure 5. As the strain increases to 0.112, PbTe experiences a linear stress response against strain both in biaxial and pure shear deformations. With increasing shear strain further, PbTe exhibits nonlinear deformation under biaxial shear loads, which seems to be affected by the compression. This leads to a lower maximum shear stress of 2.96 GPa for biaxial shear deformation than that (3.46 GPa) for pure shear deformation. The atomic structure and bond length changes were extracted, as shown in Figure S7 in the SI. The structure distorts to resist the deformation (Figure S7(b)-(c)). As the strain increases to 0.277, corresponding to the maximum shear stress, the Pb–Te bond along the *a* axis is stretched while the Pb–Te bond along the *b* axis shrinks to accommodate the deformation, which show the same trend compared with that under pure shear deformation. However, the Pb–Te bond along the *c* axis is greatly shrunk from 3.28 to 3.12 Å, which is different from the stretching Pb–Te bond (*c* axis) under pure shear load. This bond-response process can be attributed to the compression along the *c* axis. With increasing shear strain further,

the Pb–Te bond (along the *c* axis) gradually recovers to the equilibrium length while the Pb–Te bond (along the *a* axis) rapidly increases. This weakened Pb–Te bond (*a* axis) leads to the softening ionic Pb–Te framework and gives rise to the releasing shear stress from 0.277 to 0.592 shear strain (Figure 5).

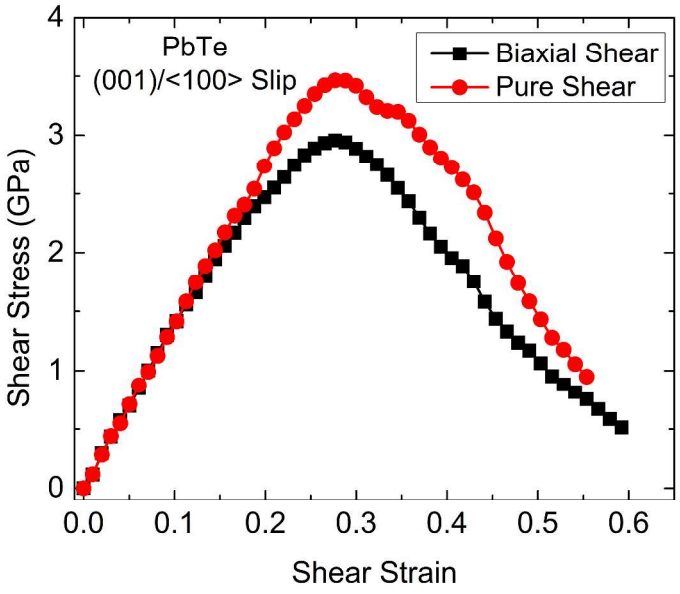

Figure 5. Computed shear-stress – shear-strain relations of PbTe under the pure shear deformation and biaxial shear deformations along the (001)/<100> direction.

3.7 Fracture Toughness Estimation from Ideal Stress-Strain Calculations

To elaborate on the structural resistance of these materials and to emphasize the relevance of these results to experiments, we estimated the fracture toughness of these chalcogenides from the ideal stress-strain curves obtained by DFT. Since fracture toughness is a metric that describes how stress is amplified at a crack tip, where fracture propagates when an applied stress is amplified beyond the strength of the molecular bond, it follows that calculation of the ideal stress-strain relations may be used to estimate the critical fracture toughness, K_c. The detailed estimation method is illustrated in the supporting information.

Considering the case of plane-strain (thick plate assumption) under mode I (see Fig. S10) deformation, the well-known Griffith-Irwin relation [43,44] takes the form:

$$K_{Ic}^2 = \frac{G_{Ic}E}{1-\nu^2} = \frac{2G_{Ic}\mu}{1-\nu} = \sigma_{gf}^2 \pi \alpha_c \quad \text{Eqn. 2}$$

Where E is the Young's modulus, μ is the shear modulus, ν is Poisson's ratio, σ_{gf} is the Griffith fracture stress for a critical crack length, α_c, and Irwin [44] called G_c the energy release rate. For brittle materials, Griffith found:

$$G_{Ic} = 2\gamma_s \quad \text{Eqn. 3}$$

where γ is the fracture surface energy and the factor of 2 arises because 2 surfaces are created. Orowan [45] and Irwin [46] generalized the Griffith result to include ductile fracture, but the form of Eqn. 2 was retained. Therefore, G_{Ic} is the work of fracture (energy of cleavage) per unit of the cross sectional area, which is just the integral under the ideal engineering tensile stress-displacement curve (Supplementary).[47] Considering the [100] loading direction of PbTe from Fig. 3, K_{Ic} is estimated to be 0.28 MPa $m^{1/2}$. This agrees with the results of Ni, et al.,[48] who reported a fracture toughness of 0.35±0.04 MPa $m^{1/2}$ for a PbTe-PbS alloy system, confirming that alloying PbTe with PbSe or PbS tends to increase the structural resistance.

Furthermore, the ideal shear stress-strain relations (Fig. 4) can be utilized to estimate the fracture toughness for mode II and III loading conditions (see Fig. S10). For mode II in the plane strain condition, Rice [49] derived:

$$K_{IIc}^2 = \frac{2G_{IIc}\mu}{1-\nu} \quad \text{Eqn. 4}$$

and from similar arguments, the mode III fracture toughness:

$$K_{IIIc}^2 = 2G_{IIIc}\mu \quad \text{Eqn. 5}$$

where $G_{IIc} = G_{IIIc} = \gamma_{us}$, which he calls the unstable stacking energy, which corresponds approximately to the energy required to nucleate a full dislocation (edge in mode II and screw in mode III). γ_{us} is similarly given by the area under the ideal engineering shear stress-displacement curves (Supplementary). Modes II and III fracture toughness was found to increase in the order

PbTe < PbSe < PbS, and the results are summarized in Table 2. This is in agreement with the structural resistance argument of the previous section.

Table 2. Fracture toughness estimations for the lead chalcogenides, and the comparison with the previous experiment.

Compound	K_{IC} (MPa $m^{1/2}$)	K_{IIC} (MPa $m^{1/2}$)	K_{IIIC} (MPa $m^{1/2}$)
PbTe	0.28	0.23	0.20
PbSe	--	0.33	0.28
PbS	--	0.41	0.35
PbTe-PbS alloy	0.35 [48]		

3.8 Fracture Toughness from Experimental Tests

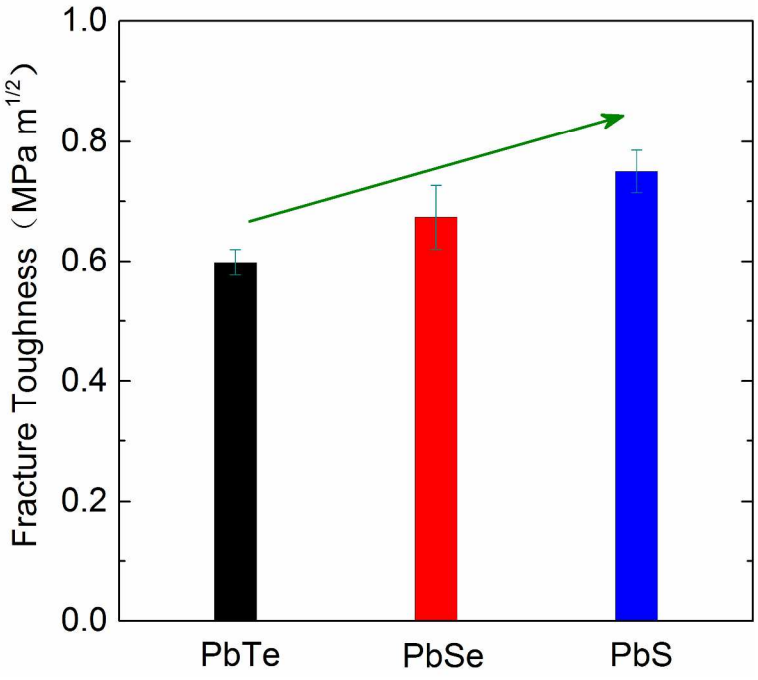

Figure 6. Fracture toughness from experimental tests for polycrystalline PbTe, PbSe and PbS. The green bars indicate the experimental error.

To further verify the fracture toughness estimation, we measured the experimental fracture toughness (K_{IC}) of Pb*X* (*X*= Te, Se, S), using the three point flexural specimen by the single-edge notch beam tests. All the XRD patterns in Figure. S11 show clearly that the single phase was

obtained for Pb*X* (*X*= Te, Se, S). As shown in Figure 6, the fracture toughness of PbTe is 0.59±0.02 MPa $m^{1/2}$, a little higher than that (0.28 MPa $m^{1/2}$) from our estimation. PbSe and PbS show a higher and much higher fracture toughness of 0.67±0.05 MPa $m^{1/2}$ and 0.75±0.04 MPa $m^{1/2}$, respectively. This trend is in good agreement with our theoretical estimation above (see section 3.7).

Here, we successfully applied the ideal stress-strain relations from DFT calculations to predict the fracture toughness, which showed good agreement with the experiment. This verifies that the investigation of the ideal stress-strain relations at the atomic scale can be used to rationally design the macroscopic mechanical properties, which is beneficial for the development of robust TE materials.

For a face centered cubic (FCC) crystal, the slip system is well known as {111} planes and <110> directions.[50] However, PbTe, which adopts a FCC structure, has the most plausible slip system of (001)/<100>. The number of Pb-Te bond along {001} planes (0.093 bond/$Å^2$, 16 bonds in lateral area of 172.24 $Å^2$ as shown in Figure 2(b)) is less than that along {111} planes (0.174 bond/$Å^2$, 26 bonds in lateral area of 149.22 $Å^2$ as shown in Figure S1(a)). This suggests that PbTe is more easily cleaved along {001} planes rather than {111} planes. Thus, in PbTe, the (001)/<100> slip system is most likely to be activated under pressure, which is similarly found in another FCC crystal, $CoSb_3$.[37]

Experimentally, alloying Pb*X* (*X* = Te, Se, S) inevitably leads to defects such as vacancies, dislocations and other modulations in the samples,[51] which would not be favorable for mechanical stability. Studying these effects requires cell sizes much larger than practical for DFT. Thus, large-scale molecular dynamics (MD) simulations will be useful for studying how such defects influence the mechanical properties of Pb*X* (*X* = Te, Se, S) alloys. This is worthy of future studies. In addition, the ferroelectric instability in PbTe, which is the origin of its low thermal conductivity,[52] is known to notably affect the crystal structure locally. Exploring the role of ferroelectric instability on the mechanical properties of PbTe requires a larger supercell as well, which will also be studied using MD simulations in the near future.

4. CONCLUSIONS

We used density functional theory (DFT) to determine the ideal strength and failure mechanism of single-crystalline PbTe. We also used the ideal structure-property relation to estimate the fracture toughness. We find that PbTe displays the lowest ideal shear strength of 3.46 GPa along the (001)/<100> slip system, which is considerably lower than the lowest ideal tensile

strength of 5.55 GPa along the [100] tension. Due to compression, PbTe has a lower ideal strength (2.96 GPa) under biaxial shear deformation. The softening and breaking of the ionic Pb−Te bond is responsible for the failure of PbTe. The estimated fracture toughness increases in the order PbTe < PbSe < PbS, which agrees well with our experimental result. To improve the mechanical strength of PbTe, we propose an alloying strategy with using isotypic PbSe or PbS to strengthen the structural stiffness of ionic Pb−Te framework. This is considered to be effective in developing robust PbTe materials for high-performance TE device applications.

ACKNOWLEDGEMENTS

This work is partially supported by National Basic Research Program of China (973-program) under Project no. 2013CB632505, the 111 Project of China under Project no. B07040. We would like to acknowledge the Jet Propulsion Laboratory, California Institute of Technology, as a funding source under a contract with the National Aeronautics and Space Administration, which was supported by the NASA Science Missions Directorate's Radioisotope Power Systems Technology Advancement Program. W.A.G was supported by DARPA W31P4Q13-1-0010.

Supporting Information. Shear deformation mechanisms of PbTe along the (111)/<1-10> and (111)/<11-2> slip systems; Tensile deformation mechanisms of PbTe along the [1-10] and [111] directions; Shear deformation mechanisms of PbSe and PbS along the (001)/<100> slip system; Biaxial shear deformation mechanism of PbTe along the (001)/<100> slip system; Estimation of fracture toughness from ideal stress-strain curves; X-ray diffraction of PbTe, PbSe and PbS samples.

REFERENCES

(1) Bell, L. E., Cooling, Heating, Generating Power, and Recovering Waste Heat with Thermoelectric Systems. *Science.* **2008**, *321*, 1457-1461.

(2) Snyder, G. J.; Toberer, E. S. Complex Thermoelectric Materials. *Nat. Mater.* **2008**, 7, 105-114.

(3) Pei, Y.; Shi, X.; LaLonde, A.; Wang, H.; Chen, L.; Snyder, G. J., Convergence of Electronic Bands for High Performance Bulk Thermoelectrics. *Nature.* **2011,** 473, 66-69.

(4) Zhao, L. D.; Dravid, V. P.; Kanatzidis, M. G., The Panoscopic Approach to High Performance Thermoelectrics. *Energ. Environ. Sci.* **2014,** *7* (1), 251-268.

(5) Chen, Z. W.; Ge, B. H.; Li, W.; Lin, S. Q.; Shen, J. W.; Chang, Y. J.; Hanus, R.; Snyder, G. J.; Pei, Y. Z., Vacancy-Induced Dislocations within Grains for High-Performance PbSe Thermoelectrics. *Nat. Commun.* **2017**, 8, 13828.

(6) Tang, Y. L.; Gibbs, Z. M.; Agapito, L. A.; Li, G.; Kim, H. S.; Nardelli, M. B.; Curtarolo, S.; Snyder, G. J., Convergence of Multi-Valley Bands as the Electronic Origin of High Thermoelectric Performance in $CoSb_3$ Skutterudites. *Nat. Mater.* **2015**, 14, 1223-1228.

(7) Tang, Y.; Hanus, R.; Chen, S. W.; Snyder, G. J., Solubility Design Leading to High Figure of Merit in Low-Cost Ce-$CoSb_3$ Skutterudites. *Nat. Commun.* **2015,** *6*, 7584.

(8) Meng, X.; Liu, Z.; Cui, B.; Qin, D.; Geng, H.; Cai, W.; Fu, L.; He, J.; Ren, Z.; Sui, J., Grain Boundary Engineering for Achieving High Thermoelectric Performance in n-Type Skutterudites. *Adv. Energy. Mater.* **2017**, 1602582.

(9) Kim, S. I.; Lee, K. H.; Mun, H. A.; Kim, H. S.; Hwang, S. W.; Roh, J. W.; Yang, D. J.; Shin, W. H.; Li, X. S.; Lee, Y. H.; Snyder, G. J.; Kim, S. W., Dense Dislocation Arrays Embedded in Grain Boundaries for High-Performance Bulk Thermoelectrics. *Science* **2015,** *348* (6230), 109-114.

(10) Poudel, B.; Hao, Q.; Ma, Y.; Lan, Y. C.; Minnich, A.; Yu, B.; Yan, X. A.; Wang, D. Z.; Muto, A.; Vashaee, D.; Chen, X. Y.; Liu, J. M.; Dresselhaus, M. S.; Chen, G.; Ren, Z. F., High-Thermoelectric Performance of Nanostructured Bismuth Antimony Telluride Bulk Alloys. *Science.* **2008,** *320* (5876), 634-638.

(11) Park, K.; Ahn, K.; Cha, J.; Lee, S.; Chae, S. I.; Cho, S. P.; Ryee, S.; Im, J.; Lee, J.; Park, S. D.; Han, M. J.; Chung, I.; Hyeon, T., Extraordinary Off-Stoichiometric Bismuth Telluride for Enhanced n-Type Thermoelectric Power Factor. *J. Am. Chem. Soc.* **2016,** *138* (43), 14458-14468.

(12) Liu, W.; Tan, X. J.; Yin, K.; Liu, H. J.; Tang, X. F.; Shi, J.; Zhang, Q. J.; Uher, C., Convergence of Conduction Bands as a Means of Enhancing Thermoelectric Performance of n-Type $Mg_2Si_{1-x}Sn_x$ Solid Solutions. *Phys. Rev. Lett.* **2012,** *108* (16), 166601.

(13) Jiang, G. Y.; He, J.; Zhu, T. J.; Fu, C. G.; Liu, X. H.; Hu, L. P.; Zhao, X. B., High Performance $Mg_2(Si,Sn)$ Solid Solutions: a Point Defect Chemistry Approach to Enhancing Thermoelectric Properties. *Adv. Func. Mater.* **2014**, 24 (24), 3776-3781.

(14) Zeier, W. G.; Schmitt, J.; Hautier, G.; Aydemir, U.; Gibbs, Z. M.; Felser, C.; Snyder, G. J., Engineering half-Heusler Thermoelectric Materials Using Zintl Chemistry. *Nat. Rev. Mater.* **2016**, 16032.

(15) Birkel, C. S.; Zeier, W. G.; Douglas, J. E.; Lettiere, B. R.; Mills, C. E.; Seward, G.; Birkel, A.; Snedaker, M. L.; Zhang, Y.; Snyder, G. J.; Pollock, T. M.; Seshadri, R.; Stucky, G. D., Rapid Microwave Preparation of Thermoelectric TiNiSn and TiCoSb Half-Heusler Compounds. *Chem. Mater.* **2012**, 24 (13), 2558-2565.

(16) El-Genk, M. S.; Saber, H. H.; Caillat, T.; Sakamoto, J. Tests Results and Performance Comparisons of Coated and Un-Coated Skutterudite Based Segmented Unicouples. *Energ. Convers. Manage.* **2006**, 47, 174-200.

(17) Zhao, D. G.; Geng, H. R.; Chen, L. D. Microstructure Contact Studies for $CoSb_3$ Thermoelectric Devices. *Int. J. Appl. Ceram. Tec.* **2012**, 9, 733-741.

(18) Hu, X.; Jood, P.; Ohta, M.; Kunii, M.; Nagase, K.; Nishiate, H.; Kanatzidis, M. G.; Yamamoto, A., Power Generation from Nanostructured PbTe-based Thermoelectrics: Comprehensive Development from Materials to Modules. *Energy. Environ. Sci.* **2016,** *9* (2), 517-529.

(19) Li, C. C.; Snyder, G. J.; Dunand, D. C., Compressive Creep Behaviour of Hot-Pressed PbTe. *Scripta. Mater.* **2017,** *134*, 71-74.

(20) Petersen, J. E.; Scolfaro, L. M.; Myers, T. H., Elastic and Mechanical Properties of Intrinsic and Doped PbSe and PbTe Studied by First-Principles. *Mater. Chem. Phys.* **2014**, 146 (3), 472-477.

(21) Ni, J. E.; Case, E. D.; Khabir, K. N.; Stewart, R. C.; Wu, C.-I.; Hogan, T. P.; Timm, E. J.; Girard, S. N.; Kanatzidis, M. G., Room Temperature Young's Modulus, Shear Modulus, Poisson's Ratio and Hardness of PbTe–PbS Thermoelectric Materials. *Mater. Sci Eng: B.* **2010**, 170 (1-3), 58-66.

(22) Gelbstein, Y.; Gotesman, G.; Lishzinker, Y.; Dashevsky, Z.; Dariel, M. P., Mechanical Properties of PbTe-Based Thermoelectric Semiconductors. *Scripta. Mater.* **2008**, 58 (4), 251-254.

(23) Gelbstein, Y.; Dashevsky, Z.; Dariel, M. P., The Search for Mechanically Stable PbTe Based Thermoelectric Materials. *J. Appl. Phys.* **2008**, 104 (3), 033702.

(24) Zlatanov, Z. K., Mechanical Properties and Structure of Gd-Doped PbTe. *Mater. Chem. Phys.* **2007**, 103 (2-3), 470-474.

(25) Cui, J. L.; Qian, X.; Zhao, X. B., Mechanical and Transport Properties of Pseudo-Binary Alloys $(PbTe)_{1-x}$–$(SnTe)_x$ by Pressureless Sintering. *J. Alloys Compds.* **2003**, 358 (1-2), 228-234.

(26) Kresse, G.; Furthmuller, J. Efficiency of ab-initio Total Energy Calculations for Metals and Semiconductors Using a Plane-Wave Basis Set. *Comp. Mater. Sci.* **1996**, 6, 15-50.

(27) Kresse, G.; Furthmuller, J. Efficient Iterative Schemes for ab initio Total-Energy Calculations Using a Plane-Wave Basis Set. *Phys. Rev. B.* **1996**, 54, 11169-11186.

(28) Kresse, G.; Joubert, D. From Ultrasoft Pseudopotentials to the Projector Augmented-Wave Method. *Phys. Rev. B.* **1999**, 59, 1758-1775.

(29) Chung, D. H. Elastic Moduli of Single-Crystal and Polycrystalline MgO. *Philos. Mag.* **1963**, 8, 833-841.

(30) Ogata, S.; Li, J.; Yip, S. Ideal Pure Shear Strength of Aluminum and Copper. *Science.* **2002**, 298, 807-811.

(31) Li, B.; Sun, H.; Chen, C., Large Indentation Strain-Stiffening in Nanotwinned Cubic Boron Nitride. *Nat. Commun.* **2014**, 5, 4965.

(32) Silvi, B.; Savin, A., Classification of Chemical Bonds Based on Topological Analysis of Electron Localization Functions. *Nature*. **1994**, *371*, 683−686.

(33) Bouad, N.; Chapon, L.; Marin-Ayral, R. M.; Bouree-Vigneron, F.; Tedenac, J. C., Neutron Powder Diffraction Study of Strain and Crystallite Size in Mechanically Alloyed PbTe. *J. Solid. State. Chem.* **2003,** *173* (1), 189-195.

(34) de Jong, M.; Chen, W.; Angsten, T.; Jain, A.; Notestine, R.; Gamst, A.; Sluiter, M.; Krishna Ande, C.; van der Zwaag, S.; Plata, J. J.; Toher, C.; Curtarolo, S.; Ceder, G.; Persson, K. A.; Asta, M., Charting the Complete Elastic Properties of Inorganic Crystalline Compounds. *Sci. data.* **2015**, 2, 150009.

(35) Vasilevskiy, D.; Masut, R. A.; Turenne, S., Thermoelectric and Mechanical Properties of Novel Hot-Extruded PbTe n-Type Material. *J. Electron Mater.* **2012,** *41* (6), 1057-1061.

(36) Madelung, O., Semiconductors: Data Handbook, 3rd edn., *Springer, Berlin Heidelberg*, **2004**, 23, 590-592.

(37) Li, G.; An, Q.; Li, W.; Goddard, W. A.; Zhai, P.; Zhang, Q.; Snyder, G. J., Brittle Failure Mechanism in Thermoelectric Skutterudite $CoSb_3$. *Chem. Mater.* **2015,** *27*, 6329-6336.

(38) Li, G.; An, Q.; Aydemir, U.; Goddard Iii, W. A.; Wood, M.; Zhai, P.; Zhang, Q.; Snyder, G. J., Enhanced Ideal Strength of Thermoelectric Half-Heusler TiNiSn by Sub-Structure Engineering. *J. Mater. Chem. A.* **2016**, 4, 14625-14636.

(39) Ogata, S.; Li, J.; Yip, S. Ideal Pure Shear Strength of Aluminum and Copper. *Science.* **2002**, 298, 807-811.

(40) Li, G.; Aydemir, U.; Wood, M.; Goddard, W. A. III.; Zhai, P.; Zhang, Q.; Snyder, G. J., Deformation Mechanisms in the High-Efficiency Thermoelectric Layered Zintl Compounds. *J. Mater. Chem. A.* **2017**, 5, 9050-9059.

(41) Li, G.; Aydemir, U.; Wood, M.; Goddard, W. A. III.; Zhai, P.; Zhang, Q.; Snyder, G. J., Ideal Strength and Deformation Mechanism in High-Efficiency Thermoelectric SnSe. *Chem. Mater.* **2017**, 29, 2382-2389.

(42) Walle, A.; Asta, M.; Ceder, G., The Alloy Theoretic Automated Toolkit: A User Guide. *Calphad.* **2002**, *26*, 539-553.

(43) Griffith, A. A., The Phenomena of Rupture and Flow in Solids. *Philosophical transactions of the royal society of london. Series A, containing papers of a mathematical or physical character.* **1921**, 221, 163-198.

(44) Irwin, G. R., Analysis of Stresses and Strains near the End of a Crack Travelling a Plane. *J. Appl. Mech.***1957**, 24, 361-364.

(45) Orowan, E., Notch, Brittleness and the Strength of Metals. *Transactions, Institution of Engineers and Shipbuilders in Scotland*, **1945**, 89, 165-215.

(46) Irwin, G. A., *Int. Congr. Appl. Mech., 9th, Unio. Brussels*. **1957**, 8, 245.

(47) Orowan, E., Energy Criteria of Fracture. *Welding Journal Research Supplement.* **1955**, 34, 1575-1605.

(48) Ni, J. E.; Case, E. D.; Khabir, K. N.; Stewart, R. C.; Wu, C.-I.; Hogan, T. P.; Timm, E. J.; Girard, S. N.; Kanatzidis, M. G., Room Temperature Young's Modulus, Shear Modulus, Poisson's Ratio and Hardness of PbTe–PbS Thermoelectric Materials. *Mater. Sci. Eng. B.* **2010**, *170*, 58-66.

(49) Rice, J. R., Dislocation Nucleation from a Crack Tip: an Analysis based on the Peierls Concept. *J. Mech. Phys. Solids.* **1992**, *40*, 239-271.

(50) Groves, G. W.; Kelly, A., Independent Slip Systems in Crystals. *Philos. Mag.* **1963**, 8 (89), 877-887.

(51) Yamini, S. A.; Wang, H.; Ginting, D.; Mitchell, D. R.; Dou, S. X.; Snyder, G. J., Thermoelectric Performance of N-Type (PbTe)0.75(PbS)0.15(PbSe)0.1 Composites. *ACS. Appl. Mater. Interfaces.* **2014,** *6* (14), 11476-11483.

(52) Zhang, Y.; Ke, X.; Kent, P. R.; Yang, J.; Chen, C., Anomalous Lattice Dynamics near the Ferroelectric Instability in PbTe. *Phys. Rev. Lett.* **2011,** *107* (17), 175503.

A TOC Figure:

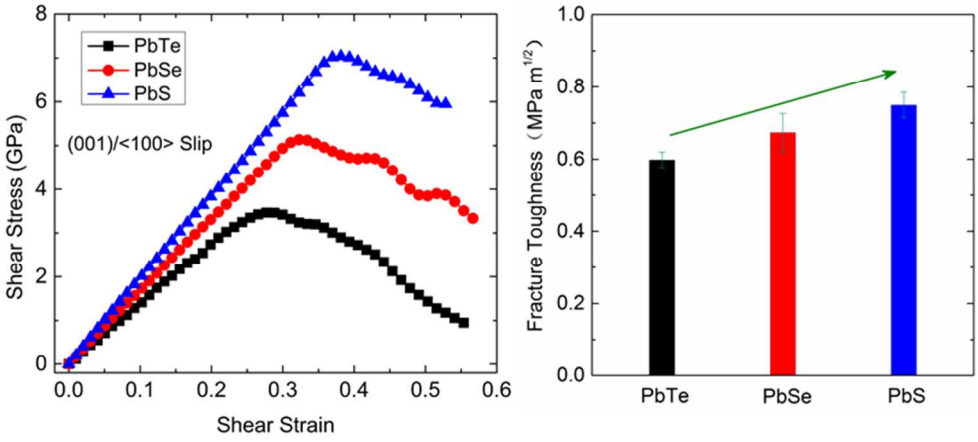
PbTe
PbSe
PbS
(001)/<100> Slip
Shear Stress (GPa)
Shear Strain
0
2
4
6
8
0.0
0.1
0.2
0.3
0.4
0.5
0.6
Fracture Toughness (MPa m^1/2)
0.0
0.2
0.4
0.6
0.8
1.0
PbTe
PbSe
PbS